Role of lysosomal channel protein TPC2 in osteoclast differentiation and bone remodeling under normal and low-magnesium conditions

Received for publication, February 15, 2017, and in revised form, September 25, 2017 Published, Papers in Press, October 30, 2017, DOI 10.1074/jbc.M117.780072

Takuya Notomi[‡§¶1], Miyuki Kuno[‖], Akiko Hiyama[¶], Tadashige Nozaki[¶], Kiyoshi Ohura[¶], Yoichi Ezura[‡], and Masaki Noda[‡§2]**

*From the [‡]Department of Molecular Pharmacology, Medical Research Institute and the [§]Global Center of Excellence Program for Molecular Science for Tooth and Bone Diseases, Tokyo Medical and Dental University, Bunkyo 113-8510, Tokyo, Japan, the [¶]Department of Pharmacology, Osaka Dental University, Hirakata, Osaka 573-1121, Japan, the [‖]Department of Physiology, Graduate School of Medicine, Osaka City University, Abeno, Osaka 545-8585, Japan, and the **Yokohama City Minato Red Cross Hospital, Yokohama, Kanagawa 231-8682, Japan*

Edited by Thomas Söllner

The bone is the main storage site for Ca^{2+} and Mg^{2+} ions in the mammalian body. Although investigations into Ca^{2+} signaling have progressed rapidly and led to better understanding of bone biology, the Mg^{2+} signaling pathway and associated molecules remain to be elucidated. Here, we investigated the role of a potential Mg^{2+} signaling-related lysosomal molecule, two-pore channel subtype 2 (TPC2), in osteoclast differentiation and bone remodeling. Previously, we found that under normal Mg^{2+} conditions, TPC2 promotes osteoclastogenesis. We observed that under low-Mg^{2+} conditions, TPC2 inhibited, rather than promoted, the osteoclast differentiation and that the phosphatidylinositol 3,5-bisphosphate ($PI(3,5)P_2$) signaling pathway played a role in the TPC2 activation under low-Mg^{2+} conditions. Furthermore, $PI(3,5)P_2$ depolarized the membrane potential by increasing the intracellular Na^+ levels. To investigate how membrane depolarization affects osteoclast differentiation, we generated a light-sensitive cell line and developed a system for the light-stimulated depolarization of the membrane potential. The light-induced depolarization inhibited the osteoclast differentiation. We then tested the effect of *myo*-inositol supplementation, which increased the $PI(3,5)P_2$ levels in mice fed a low-Mg^{2+} diet. The *myo*-inositol supplementation rescued the low-Mg^{2+} diet–induced trabecular bone loss, which was accompanied by the inhibition of osteoclastogenesis. These results indicate that low-Mg^{2+}–induced osteoclastogenesis involves changes in the role of TPC2, which are mediated through the $PI(3,5)P_2$ pathway. Our findings also suggest that *myo*-inositol consumption might provide beneficial effects in Mg^{2+} deficiency–induced skeletal diseases.

Ca^{2+} is recognized as a necessary factor for bone health, and the calcium signaling pathway has been extensively studied in the bone. However, other minerals, including zinc, copper, and magnesium, are also known to be critical for bone health (1, 2). In particular, bones are known to store >50% of the total Mg^{2+} in the body (3, 4), and Mg^{2+} deficiency causes bone loss, coupled with an increase in osteoclastogenesis (5, 6). However, the underlying intracellular molecular pathway and associated molecules required for osteoclastogenesis remain unidentified.

The mechanism of osteoclastogenesis has been extensively investigated (7–10). Previous studies have shown that the receptor activator of nuclear factor-κB (RANK)/RANK ligand (RANKL)[3] pathway induces changes in intracellular Ca^{2+} ($[Ca^{2+}]_i$) levels. This leads to Ca^{2+}/calcineurin-dependent dephosphorylation and activation of NFATc1 (nuclear factor of activated T cells 1), which translocates from the cytosol to the nucleus (9, 10). With regard to osteoclastic molecules associated with the $[Ca^{2+}]_i$ pathway, we have previously reported that a lysosomal Ca^{2+} channel, two-pore channel subtype 2 (TPC2), functions in osteoclastogenesis (10).

TPC2 is a member of a newly identified family of Ca^{2+}-permeable channels, which is activated by nicotinic acid adenine dinucleotide phosphate (NAADP), a potent Ca^{2+}-mobilizing cellular messenger (11, 12). TPC2 has been identified as a lysosomal Ca^{2+} channel, and thus it does not localize in the endosome, endoplasmic reticulum, Golgi apparatus, or mitochon-

This work was supported in part by grants from the Uehara Memorial Foundation, the Nakatomi Foundation, and the Naito Foundation and by Japan Society for the Promotion of Science Grants KAKENHI 24119505, 25670638, 26282182, 26253085, 15K15558, and 16K15655. The authors declare that they have no conflicts of interest with the contents of this article.

This article contains supplemental Figs. S1–S3.

[1] To whom correspondence may be addressed: Dept. of Molecular Pharmacology, Medical Research Institute, Tokyo Medical and Dental University, 1-5-45 Yushima, Bunkyo 113-8510, Tokyo, Japan. Tel: 81-72-864-3058; Fax: 81-72-864-3158; E-mail: notomi@cc.osaka-dent.ac.jp.

[2] To whom correspondence may be addressed: Dept. of Molecular Pharmacology, Medical Research Institute, Tokyo Medical and Dental University, 1-5-45 Yushima, Bunkyo 113-8510, Tokyo, Japan. Tel. and Fax: 81-3-5803-4061; E-mail: noda.mph@mri.tmd.ac.jp.

[3] The abbreviations used are: RANK, receptor activator of nuclear factor-κB; RANKL, RANK ligand; TPC2, two-pore channel subtype 2; $PI(3,5)P_2$, phosphatidylinositol 3,5-bisphosphate; NAADP, nicotinic acid adenine dinucleotide phosphate; BM, bone marrow; TRAP, tartrate-resistant acid phosphatase; PIKfyve, FYVE-finger–containing phosphoinositide kinase; $PI(3,5)P_2$+C3, $PI(3,5)P_2$ with Carrier3; PBS+C3, PBS with Carrier3; WR, channel rhodopsin-wide receiver—mCherry; NMg, normal-Mg^{2+} diet; Ino, *myo*-inositol; NMg+Ino, normal-Mg^{2+} diet with *myo*-inositol; LMg, low-Mg^{2+} diet; LMg+Ino, low-Mg^{2+} diet with *myo*-inositol; BV/TV, bone volume/tissue volume ratio; Oc.S/BS, osteoclast surface area/bone surface area ratio; Oc.N/BS, osteoclast number/bone surface ratio; HBSS, Hanks' balanced salt solution; BM-OC, bone marrow-derived osteoclast.

dria. NAADP evokes Ca^{2+} release through TPC2 from the lysosome (11), and this leads to further Ca^{2+} release from the endoplasmic reticulum through inositol triphosphate receptors or ryanodine receptors (11, 12). In relation to bone biology, we have identified TPC2 as a previously unknown regulator of osteoclastogenesis. We have shown that in the RANK/RANKL pathway, TPC2 promotes osteoclast differentiation through changes in $[Ca^{2+}]_i$ and NFATc1 localization (10). However, other studies have demonstrated that TPC2 is a phosphatidylinositol 3,5-bisphosphate ($PI(3,5)P_2$)-activated sodium channel (13–15). Notably, NAADP failed to activate TPC2 in enlarged lysosomes; however, a $PI(3,5)P_2$-activated Na^+ current was recorded and shown to be inhibited in TPC2-deficient cells (13). To explain this discrepancy, a previous study has suggested that changes in Mg^{2+} concentrations can potentially induce a functional conversion of TPC2 from a NAADP-activated channel to a $PI(3,5)P_2$-stimulated channel (16).

The aforementioned finding led us to investigate whether osteoclastic TPC2 is associated with low-Mg^{2+}–induced osteoclastogenesis and bone loss. Here, we present the results showing that TPC2 plays a different role under low-Mg^{2+} conditions and inhibits osteoclastogenesis through $PI(3,5)P_2$-dependent changes in $[Na^+]_i$ but not in $[Ca^{2+}]_i$. This role of the channel is functionally the opposite of that revealed by our previous findings, which showed that TPC2 normally promotes osteoclastogenesis (10). We further report here that *myo*-inositol supplementation, which increases the $PI(3,5)P_2$ levels, rescued the low-Mg^{2+}–induced bone loss by reducing osteoclastogenesis.

Results

TPC2 negatively regulates low-Mg^{2+}–induced osteoclastogenesis

To confirm the effects of low Mg^{2+} on osteoclast differentiation, we used Mg^{2+}-free DMEM as the culture medium and included only 2.5% FBS in the culture medium to eliminate as much Mg^{2+} as possible. In this culture medium, the Mg^{2+} concentration was considerably lower than that in the control medium (supplemental Fig. S1*A*). We hypothesized that osteoclastic TPC2 was functionally affected under low-Mg^{2+} conditions (supplemental Fig. S3*B*). To confirm that the extracellular Mg^{2+} concentration affects the intracellular Mg^{2+} concentration, we performed two experiments. Based on the biochemical analysis of cell lysates, a low extracellular concentration of Mg^{2+} decreased the concentration of Mg^{2+} in the cell (Fig. 1*A*). Next, analysis of Mg^{2+} imaging revealed that changes in extracellular Mg^{2+} from 1 to 0 mM gradually decreased the Mg^{2+} fluorescence intensity of RAW 264.7 cells (supplemental Fig. S1, *B* and *C*). These results suggested that the cytosolic concentration of Mg^{2+} changed depending on the extracellular Mg^{2+} concentration. In the low-Mg^{2+} culture medium, osteoclast differentiation was promoted in stromal cell-free bone marrow (BM) and RAW 264.7 mouse osteoclast precursor-like cells (RAW) (Fig. 1, *B versus D* and *G*, and supplemental Fig. S1*F*). To investigate the role of TPC2 in osteoclast differentiation, we used TPC2-WT and TPC2 deletion BM and RAW cells. The TPC2 protein was detected in TPC2-WT BM and RAW cells, whereas the bands were not detected upon TPC2 deletion (Fig. 1*F* and supplemental Fig. S1*D*). To confirm the antibody specificity, the antibody was preincubated with the antigen, and no bands were detected (supplemental Fig. S1*E*). Thus, this antibody was concluded to bind to the TPC2 protein. Under normal-Mg^{2+} conditions, the deletion of TPC2 inhibited osteoclast differentiation, as determined by the activity of tartrate-resistant acid phosphatase (TRAP) (Fig. 1*G* and supplemental Fig. S1*F*), similar to a previous report on TPC2 knockdown cells (10). However, in a low-Mg^{2+} culture, the deletion of TPC2 promoted osteoclast differentiation (Fig. 1, *D versus E* and *G*, and supplemental Fig. S1*F*). These effects on osteoclastogenesis were also confirmed based on the mRNA expression of osteoclast differentiation markers (calcitonin receptor, integrin β3, and cathepsin K; Fig. 1, *H–J*, and supplemental Fig. S1, *G–I*).

To further confirm that TPC2 plays a role in osteoclastogenesis under low-Mg^{2+} conditions, a TPC2 inhibitor, Ned19, was added to the culture medium. Whereas inhibition of TPC2 decreased the TRAP activity and mRNA expression of osteoclast differentiation markers under normal-Mg^{2+} conditions (Fig. 1, *K–N*, and supplemental Fig. S1, *J–M*), those values were increased in the presence of Ned19 under low-Mg^{2+} conditions (Fig. 1, *K–N*, and supplemental Fig. S1, *J–M*). These results suggested that the role of TPC2 changed in the low-Mg^{2+} culture medium. To investigate this change, we focused on another TPC2 ligand, $PI(3,5)P_2$ (13–15). The enzyme FYVE-finger–containing phosphoinositide kinase (PIKfyve) phosphorylates phosphatidylinositol 3-phosphate to generate $PI(3,5)P_2$. First, we examined the effect of the PIKfyve inhibitor YM201636 on osteoclast development and found that inhibition of PIKfyve only had an effect in the low-Mg^{2+} culture medium (Fig. 1, *O–R*, and supplemental Fig. S1, *N–Q*). Next, to investigate the direct role of $PI(3,5)P_2$ in osteoclastogenesis, $PI(3,5)P_2$ with Carrier3 ($PI(3,5)P_2$+C3) was added to cells by using a shuttle PIP kit. The $PI(3,5)P_2$+C3 addition affected osteoclast differentiation only under the low-Mg^{2+} condition (Fig. 1, *S–V*, and supplemental Fig. S1, *R–U*), and the effect was diminished in TPC2 deletion cells (Fig. 1*W* and supplemental Fig. S1*V*). These findings indicated that the TPC2 activity was mediated via the $PI(3,5)P_2$ signaling pathway only under the low-Mg^{2+} condition.

$PI(3,5)P_2$ increases $[Na^+]_i$ and depolarizes the cell membrane potential under low-Mg^{2+} conditions in osteoclast-like cells

To investigate the signaling pathway responsible for the negative effects of $PI(3,5)P_2$ on osteoclast differentiation under the low-Mg^{2+} condition, we measured changes in intracellular ion levels using fluorescent dyes. For this purpose, we used the TPC2-WT and gene-edited (TPC2 deletion) RAW cell lines. $PI(3,5)P_2$ is a TPC2 ligand generating a Na^+ current (13, 15) but not a Ca^{2+} current. In both TPC2-WT and TPC2-deletion cells, $PI(3,5)P_2$+C3 showed no effects on relative fluorescence of the dye specific for $[Ca^{2+}]_i$, under normal- and low-Mg^{2+} conditions (Fig. 2, *A–D*). To reliably confirm the data of the $[Ca^{2+}]_i$ measurements, ATP with Carrier3 was added, which

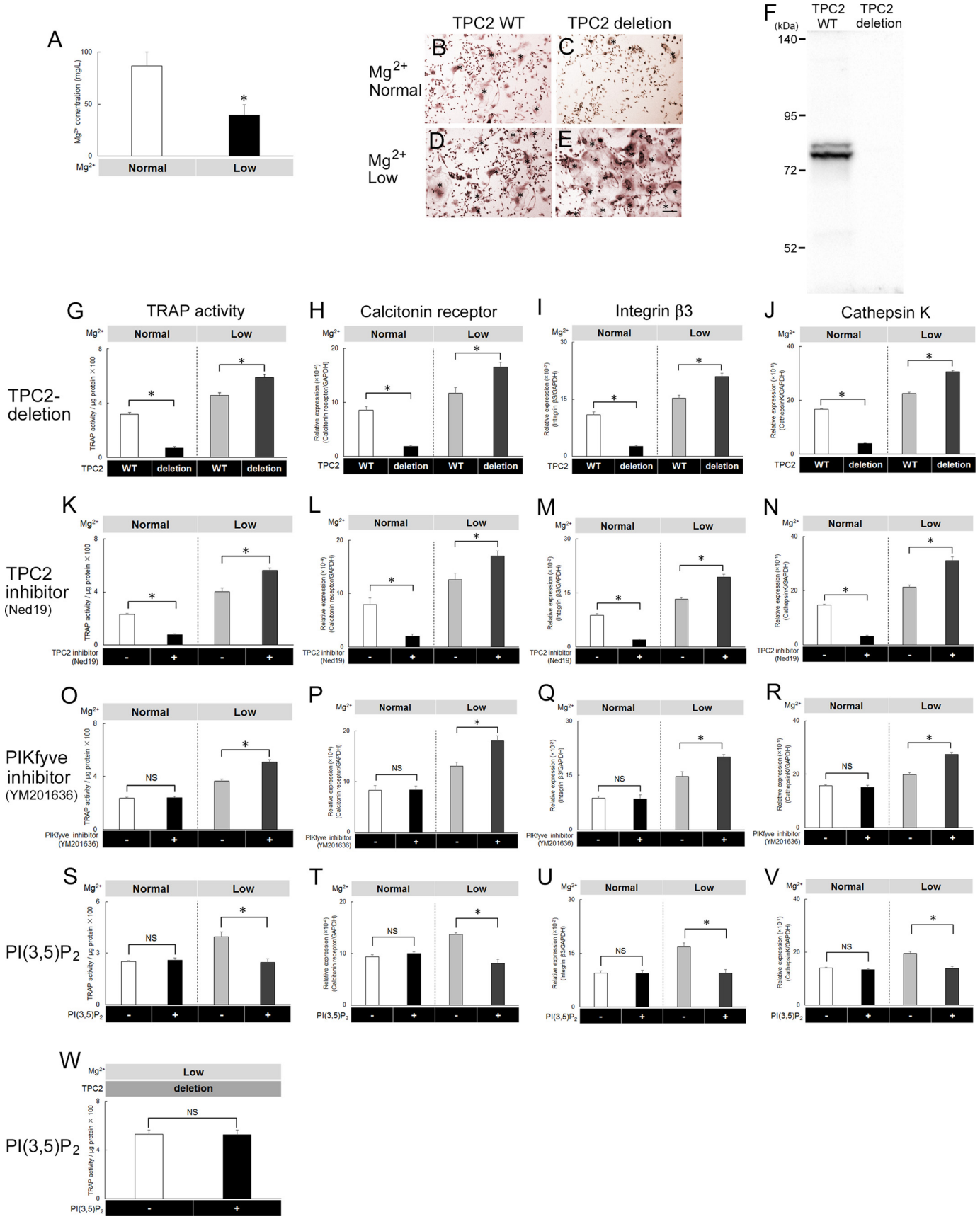
A
Mg2+ concentration (mg/L)
100
50
0
Mg2+
Normal
Low
TPC2 WT
TPC2 deletion
B
C
D
E
Mg2+ Normal
Mg2+ Low
F
(kDa)
TPC2 WT
TPC2 deletion
140
95
72
52
G
TRAP activity
H
Calcitonin receptor
I
Integrin β3
J
Cathepsin K
TPC2-deletion
Mg2+
Normal
Low
TPC2
WT
deletion
TRAP activity / μg protein × 100
Relative expression (×10-4) (Calcitonin receptor/GAPDH)
Relative expression (×10-2) (Integrin β3/GAPDH)
Relative expression (×10-1) (CathepsinK/GAPDH)
K
L
M
N
TPC2 inhibitor (Ned19)
TPC2 inhibitor (Ned19)
-
+
O
P
Q
R
PIKfyve inhibitor (YM201636)
PIKfyve inhibitor (YM201636)
NS
S
T
U
V
PI(3,5)P2
PI(3,5)P2
W
PI(3,5)P2
Low
deletion

resulted in increases in the fluorescence intensity and amplitude (supplemental Fig. S2*F*). By contrast, the $PI(3,5)P_2$+C3 addition increased relative fluorescence of the dye specific for $[Na^+]_i$ (Fig. 2*E*). At 120 min after the addition of $PI(3,5)P_2$+C3, relative fluorescence of the dye specific for $[Na^+]_i$ increased under both normal- and low-Mg^{2+} conditions (Fig. 2, *E* and *G*); however, the $PI(3,5)P_2$-induced increase in $[Na^+]_i$ was considerably higher under the low-Mg^{2+} condition (Fig. 2*G*). Notably, this $[Na^+]_i$ increase was diminished in TPC2-deletion cells (Fig. 2, *F* and *H*). To confirm that the fluorescence signal is due to Na^+ influx, NaCl was replacement by *N*-methyl-D-glucamine chloride. Addition of $PI(3,5)P_2$+C3 increased relative fluorescence; however, its increment was little in the replacement of NaCl by *N*-methyl-D-glucamine chloride (supplemental Fig. S2*G*). This suggests that the signal is mainly due to Na^+ influx. Next, we focused on the change in the membrane potential caused by the $[Na^+]_i$ increase. Using a fluorescent dye specific for the cell membrane potential, we determined that the membrane potential gradually increased after $PI(3,5)P_2$+C3 addition only under the low-Mg^{2+} condition (Fig. 2, *I* and *K*). However, no increase was observed in TPC2-deletion cells (Fig. 2, *J* and *L*). These results suggested that $PI(3,5)P_2$ depolarized the cell membrane potential through TPC2 and depolarization occurred only under low-Mg^{2+} conditions. After the addition of PBS with Carrier3 (PBS+C3) in normal- and low-Mg^{2+} culture medium, the relative fluorescence of Na^+ gradually increased. At 120 min after the addition, the relative fluorescence changes in the $[Na^+]_i$ ($\Delta[Na^+]_i$) was 10.2 ± 0.7 ($n = 5$) for normal-Mg^{2+} culture medium and 10.5 ± 0.5 ($n = 5$) for low-Mg^{2+} culture medium. The Mg^{2+} concentrations did not affect the values. However, the increases by $PI(3,5)P_2$+C3 were significantly larger than those induced by PBS+C3 and were dependent on Mg^{2+} concentration. These data confirmed that $PI(3,5)P_2$ increased $[Na^+]_i$ significantly in low-Mg^{2+} culture medium. In addition to these results, the deletion of TPC2 showed no effect on the Na^+ levels or membrane potential under both normal and low-Mg^{2+} conditions (Fig. 2, *E–H*), although it showed a functional effect on osteoclastogenesis (Fig. 1, *G–J*). To elucidate this inconsistency, we investigated whether RANKL affected the level of $PI(3,5)P_2$. After confirming the linearity of the signal intensity for $PI(3,5)P_2$ (supplemental Fig. S2, *H* and *I*), we quantified the $PI(3,5)P_2$ levels. At 48 h after the RANKL addition, the levels of $PI(3,5)P_2$ were higher than those in the control (supplemental Fig. S2*J*). This suggests that RANKL affects the Na^+ levels, partly via changes in $PI(3,5)P_2$ levels.

Membrane depolarization inhibits osteoclast differentiation

$PI(3,5)P_2$ inhibited osteoclastogenesis and depolarized the membrane potential. Previously, we have confirmed that membrane hyperpolarization promotes osteoclast differentiation (2). Thus, we tested our additional hypothesis, suggesting that membrane depolarization would affect osteoclastogenesis. To allow a non-invasive control of the membrane potential, we generated a RAW cell line that stably expressed the channel rhodopsin-wide receiver–mCherry (WR), which is activated by blue light and depolarizes cells through a cation influx (17). Light-induced changes in the membrane potential were recorded under the whole-cell clamp configuration in WR-expressing and control (expressing mCherry only) RAW cells. WR-expressing cells were immediately depolarized (by 29 ± 3.7 mV) upon the onset of light stimulation and returned to the prestimulus potential after termination of the stimulus (Fig. 3, *A* and 3*B*). Whereas all recorded WR-expressing cells were depolarized by the light stimulus (Fig. 3*D*), control cells did not respond to the stimulation (Fig. 3, *C* and *E*). Thus, temporal patterns of membrane depolarization could be strictly controlled using this system, which we next employed to investigate how membrane depolarization affects osteoclast differentiation. Light stimulation decreased the TRAP activity in WR-expressing cells but not in control cells (Fig. 3*F*), which indicated that osteoclast differentiation is inhibited by membrane depolarization in the presence of RANKL. To investigate the relationship between membrane depolarization and TPC2, WR was expressed in TPC2-WT and TPC2-deletion RAW 264.7 cells. The light-induced membrane depolarization reduced the TRAP activity in TPC2-WT and TPC2-deletion cells under both normal Mg^{2+} (Fig. 3*G*) and low-Mg^{2+} conditions (Fig. 3*H*). Although in the latter case, the level of TRAP activity in the TPC2-deletion cells was similar to that in the TPC2-WT cells subjected to light stimulation (Fig. 3*H*), these TPC2-related differences were unclear. These effects on osteoclast differentiation were identical to those observed upon the addition of a TPC2 inhibitor (Fig. 3, *I* and *J*). The results indicated that TPC2 was not involved in the inhibition of osteoclastogenesis under low-Mg^{2+} conditions, which was caused by light-induced membrane depolarization.

Figure 1. Low extracellular Mg^{2+} concentration affects the role of TPC2 in osteoclast differentiation. *A*, Mg^{2+} concentrations in cell lysates from a normal- or low-Mg^{2+} culture medium, measured 1 day after replacing the culture medium ($n = 4$). *, $p < 0.01$. *B–E*, representative images of Mg^{2+}-dependent osteoclast differentiation in TPC2-WT and TPC2-deletion bone marrow-derived osteoclasts (BM-OCs) 7 days after the addition of RANKL. The TPC2 deletion normally inhibited the osteoclast differentiation (*B versus C*) but promoted it under low-Mg^{2+} conditions (*D versus E*) (normal/low Mg^{2+}: Mg^{2+}-free DMEM containing 2.5% FBS with/without 1 mM $MgCl_2$, respectively). *Asterisks* show multinucleated osteoclasts. *Scale bar*, 100 μm. *F*, TPC2 protein levels were diminished by targeting the TPC2 gene in BM by clustered regularly interspaced short palindromic repeats (CRISPR)/caspase-9 (CAS9). *TPC2 WT*, non-targeted by CRISPR/CAS9; *TPC2 deletion*, TPC2 gene targeted by CRISPR/CAS9. *G–J*, TRAP activity (*G*) and mRNA expression of the calcitonin receptor (*H*), integrin β3 (*I*), and cathepsin K (*J*) in TPC2-WT and TPC2-deletion BM-OCs in normal- and low-Mg^{2+} culture media at 5 days after the addition of RANKL ($n = 9$). *, $p < 0.01$. *K–N*, TRAP activity (*K*) and mRNA expression of the calcitonin receptor (*L*), integrin β3 (*M*), and cathepsin K (*N*) in BM-OCs cultured in the presence (+) or absence (−) of the TPC2 inhibitor Ned19 in normal- or low-Mg^{2+} culture medium, measured at 5 days after the addition of RANKL ($n = 9$). *, $p < 0.01$. *O–R*, TRAP activity (*O*) and mRNA expression of the calcitonin receptor (*P*), integrin β3 (*Q*), and cathepsin K (*R*) in BM-OCs cultured in the presence (+) or absence (−) of the PIKfyve inhibitor YM201636 in normal- or low-Mg^{2+} culture medium, measured at 5 days after the addition of RANKL ($n = 9$). *, $p < 0.01$; *NS*, not significant. *S–V*, TRAP activity (*S*) and mRNA expression of the calcitonin receptor (*T*), integrin β3 (*U*), and cathepsin K (*V*) in BM-OCs cultured in the presence (+, addition of $PI(3,5)P_2$+C3) or absence (−, addition of PBS+C3) of $PI(3,5)P_2$ in normal- or low-Mg^{2+} culture medium, measured at 5 days after the addition of RANKL ($n = 9$). *, $p < 0.01$; *NS*, not significant. *W*, TRAP activity in TPC2-deficient BM-OCs in the presence (+, addition of $PI(3,5)P_2$+C3) or absence (−, addition of PBS+C3) of $PI(3,5)P_2$ in low-Mg^{2+} medium, measured at 5 days after the addition of RANKL ($n = 9$).

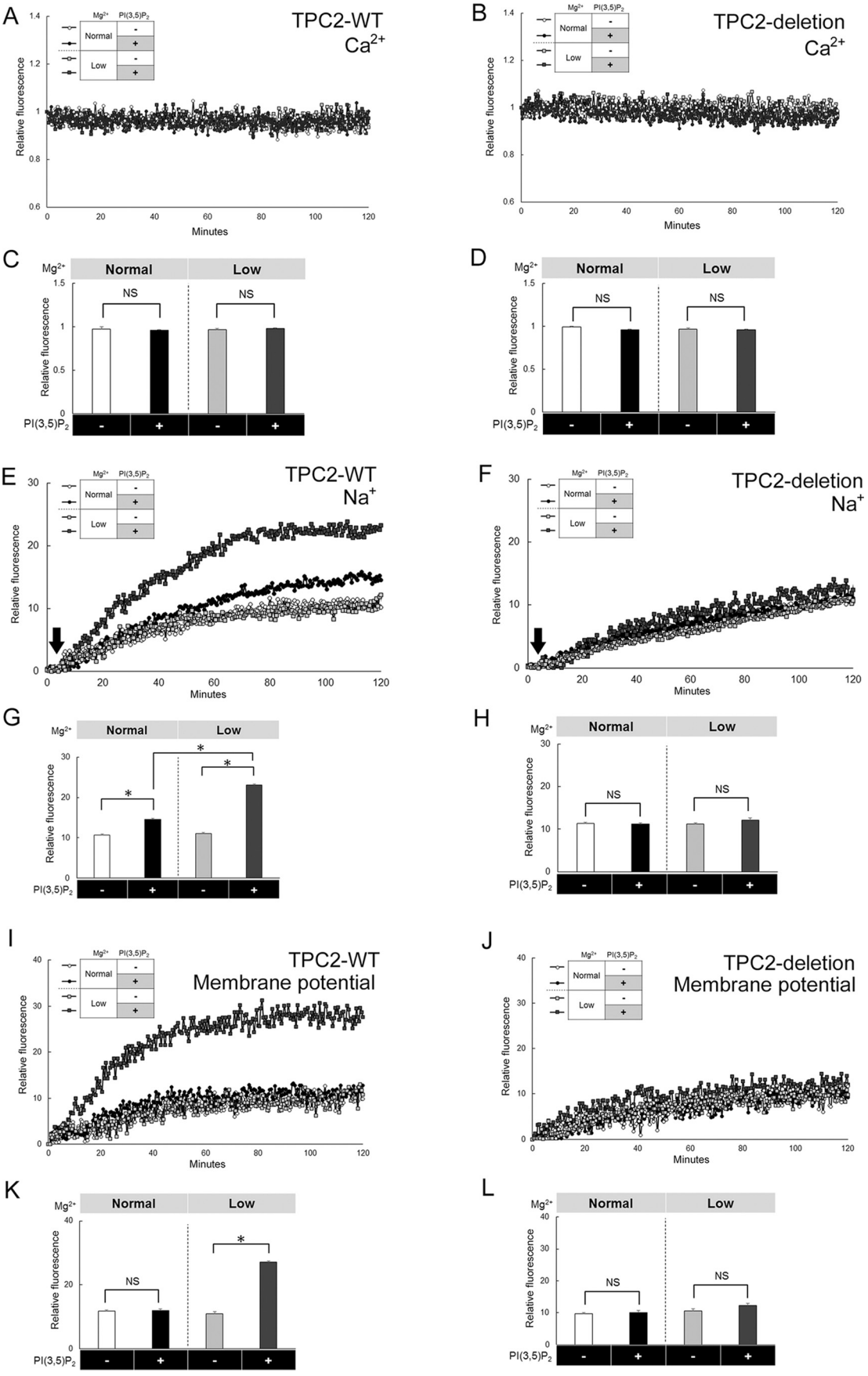
A
TPC2-WT
Ca^{2+}
B
TPC2-deletion
Ca^{2+}
Relative fluorescence
Minutes
Mg^{2+}
$PI(3,5)P_2$
Normal
Low
C
D
NS
E
TPC2-WT
Na^+
F
TPC2-deletion
Na^+
G
H
*
I
TPC2-WT
Membrane potential
J
TPC2-deletion
Membrane potential
K
L

myo-Inositol supplementation rescues bone loss induced by low-Mg^{2+} diet

Our results thus far suggested that $PI(3,5)P_2$ potentially reduced the low-Mg^{2+}–induced bone loss through inhibition of osteoclast differentiation. Various foods contain *myo*-inositol, which is commonly used as a supplement (18). Moreover, *myo*-inositol is one of the stereoisomers of inositol, and it is phosphorylated by PI3K into phosphatidylinositol 3-phosphate, which is further phosphorylated by PIKfyve to $PI(3,5)P_2$ (19). Thus, we hypothesized that *myo*-inositol supplementation could increase $PI(3,5)P_2$ and affect bone remodeling under low-Mg^{2+} conditions. To test this hypothesis, we conducted *in vitro* experiments as well as *in vivo* experiments, in which we combined a low-Mg^{2+} diet and *myo*-inositol supplementation. First, changes in $PI(3,5)P_2$ levels were investigated in RAW cells with/without *myo*-inositol addition. The results of the dot-blot analysis showed that *myo*-inositol increased the $PI(3,5)P_2$ levels at 24 h after the addition (Fig. 4*A*). To confirm the effects of *myo*-inositol on osteoclast differentiation, *myo*-inositol was added into the culture medium under the normal- or low-Mg^{2+} conditions. The TRAP activity decreased following the *myo*-inositol addition under the low-Mg^{2+} conditions but not under the normal-Mg^{2+} conditions (Fig. 4*B*), which were similar to what was observed in the experiment used to examine the effects of $PI(3,5)P_2$ (Fig. 1*S* and supplemental Fig. S1*R*). Moreover, the $PI(3,5)P_2$ levels increased in the total protein extracted from the entire tibia of the mice following the *myo*-inositol supplementation (supplemental Fig. S3*A*), as was observed in the experiments on RAW cells. The intake of water with/without *myo*-inositol did not differ among the four groups tested, normal-Mg^{2+} diet (NMg), normal-Mg^{2+} diet with *myo*-inositol (NMg+Ino), low-Mg^{2+} diet (LMg), and low-Mg^{2+} diet with *myo*-inositol (LMg+Ino) and was as follows (g/mouse/day): NMg, 5.5 ± 0.6; NMg+Ino, 5.9 ± 0.5; LMg, 5.8 ± 0.6; and LMg+Ino, 5.4 ± 0.3. The serum Mg^{2+} levels were decreased by the intake of the low-Mg^{2+} diet; however, supplementation of *myo*-inositol did not affect the serum Mg^{2+} levels in the groups fed either the normal- or low-Mg^{2+} diet (Fig. 4*C*). The low-Mg^{2+} diet–induced trabecular bone loss (Fig. 4*D*), deterioration of the trabecular structure (Fig. 4, *E–G*), and increased bone resorption (Fig. 4, *H* and *I*). In the mice fed the normal-Mg^{2+} diet (NMg *versus* NMg+Ino), *myo*-inositol supplementation did not affect the structural parameters such as the bone volume/tissue volume ratio (BV/TV; Fig. 4*D*), trabecular thickness (Tb.Th; Fig. 4*E*), trabecular number (Tb.N; Fig. 4*F*), and trabecular separation (Tb.Sp; Fig. 4*G*) or the bone resorption parameters such as the osteoclast surface area/bone surface area (Oc.S/BS) and osteoclast number/bone surface (Oc.N/BS) ratios (Fig. 4, *H* and *I*). By contrast, in the mice fed the low-Mg^{2+} diet (LMg *versus* LMg+Ino), *myo*-inositol supplementation increased BV/TV, Tb.Th, and Tb.N and decreased Tb.Sp (Fig. 4, *E–G*). Moreover, the low-Mg^{2+} diet–induced increase in the bone resorption parameters, Oc.S/BS and Oc.N/BS, was inhibited following the *myo*-inositol supplementation (Fig. 4, *H* and *I*). These results suggested that *myo*-inositol supplementation reversed the low-Mg^{2+}–induced trabecular bone loss and inhibited the low-Mg^{2+}–induced osteoclastogenesis.

Discussion

Bones store >50% of the total Mg^{2+} of the body, and osteoclasts release Mg^{2+} from the bone during bone resorption. Mg^{2+} deficiency is considered to promote osteoclastogenesis and bone loss (3, 5), but the underlying molecular pathways and associated molecules remain mostly unknown. This study demonstrated that TPC2 negatively regulated the low-Mg^{2+}–induced osteoclastogenesis through a Mg^{2+}-dependent pathway (supplemental Fig. S3*B*). Furthermore, $PI(3,5)P_2$ inhibited the osteoclast differentiation through TPC2 and membrane potential changes only under low-Mg^{2+} conditions. Accordingly, *myo*-inositol supplementation, which increased the $PI(3,5)P_2$ levels, rescued the low-Mg^{2+} diet–induced trabecular bone loss and inhibited osteoclastogenesis.

TPC2 was initially identified as a lysosomal NAADP-activated Ca^{2+} channel (11). Although numerous studies have suggested that TPC2 is related to NAADP and $[Ca^{2+}]_i$ in various cells (10, 11, 20, 21), recent reports have confirmed that TPC2 is a $PI(3,5)P_2$-activated Na^+ channel (13–15). A previous study has provided insights into the mechanism of this discrepancy, suggesting that TPC2 is functionally converted in a Mg^{2+}- and MAPK-dependent manner (16). In our previous report, we found that TPC2 promotes osteoclastogenesis through changes in $[Ca^{2+}]_i$; however, the effects of $PI(3,5)P_2$ were not examined (10). Here, we focused on functional attributes of TPC2 under low-Mg^{2+} conditions and found that TPC2 inhibited osteoclast differentiation through $PI(3,5)P_2$ signaling. Although the direct effects of Mg^{2+} on TPC2 were not elucidated in this study, our new findings provide additional insights, which can help resolve the controversy surrounding TPC2 and phospholipids. Further, low Mg^{2+} does not affect osteoclastogenesis and/or bone mass directly via TPC2 because the effect of low Mg^{2+} on osteoclastogenesis was much more profound than that observed in the presence of TPC2 under conditions of TPC2 deficiency (Fig. 1). Thus, low Mg^{2+} appears to indirectly activate a functional effect of TPC2, which counteracts the bone loss induced by low Mg^{2+}.

It is estimated that ~4–5 mM of $[Mg^{2+}]_i$ in the cytosol exists as a complex with ATP in several types of mammalian cells (22). In a previous report (23), carbonyl cyanide *p*-(trifluorome-

Figure 2. $PI(3,5)P_2$+C3 addition increases intracellular Na^+ levels and depolarizes the cell membrane potential through TPC2 under low-Mg^{2+} conditions. *A* and *B*, representative $[Ca^{2+}]_i$ plots obtained for RAW cells incubated with PBS+C3 (*white circle* and *light gray square*) or $PI(3,5)P_2$+C3 (*black circle* and *dark gray square*) in normal- or low-Mg^{2+} culture medium. *A*, TPC2-WT; *B*, TPC2 deletion. *C* and *D*, relative fluorescence of the dye specific for $[Ca^{2+}]_i$ at 120 min after the addition of PBS+C3 or $PI(3,5)P_2$+C3 ($n = 5$). *C*, TPC2-WT; *D*, TPC2 deletion. *NS*, not significant. *E* and *F*, representative $[Na^+]_i$ plots obtained for RAW cells incubated with PBS+C3 or $PI(3,5)P_2$+C3 in normal- or low-Mg^{2+} culture medium. *E*, TPC2-WT; *F*, TPC2 deletion. The *arrows* indicate the addition of PBS+C3 or $PI(3,5)P_2$+C3. *G* and *H*, relative fluorescence of the dye specific for $[Na^+]_i$ at 120 min after the addition of PBS+C3 or $PI(3,5)P_2$+C3 ($n = 5$). *G*, TPC2-WT; *H*, TPC2 deletion. *, $p < 0.01$. *NS*, not significant. *I* and *J*, representative membrane potential plots obtained for RAW cells incubated with PBS+C3 or $PI(3,5)P_2$+C3 in normal- or low-Mg^{2+} culture medium. *I*, TPC2-WT; *J*, TPC2 deletion. *K* and *L*, relative fluorescence of the dye specific for membrane potential at 120 min after the addition of PBS+C3 or $PI(3,5)P_2$+C3 ($n = 5$). *K*, TPC2-WT; *L*, TPC2 deletion. *, $p < 0.01$.

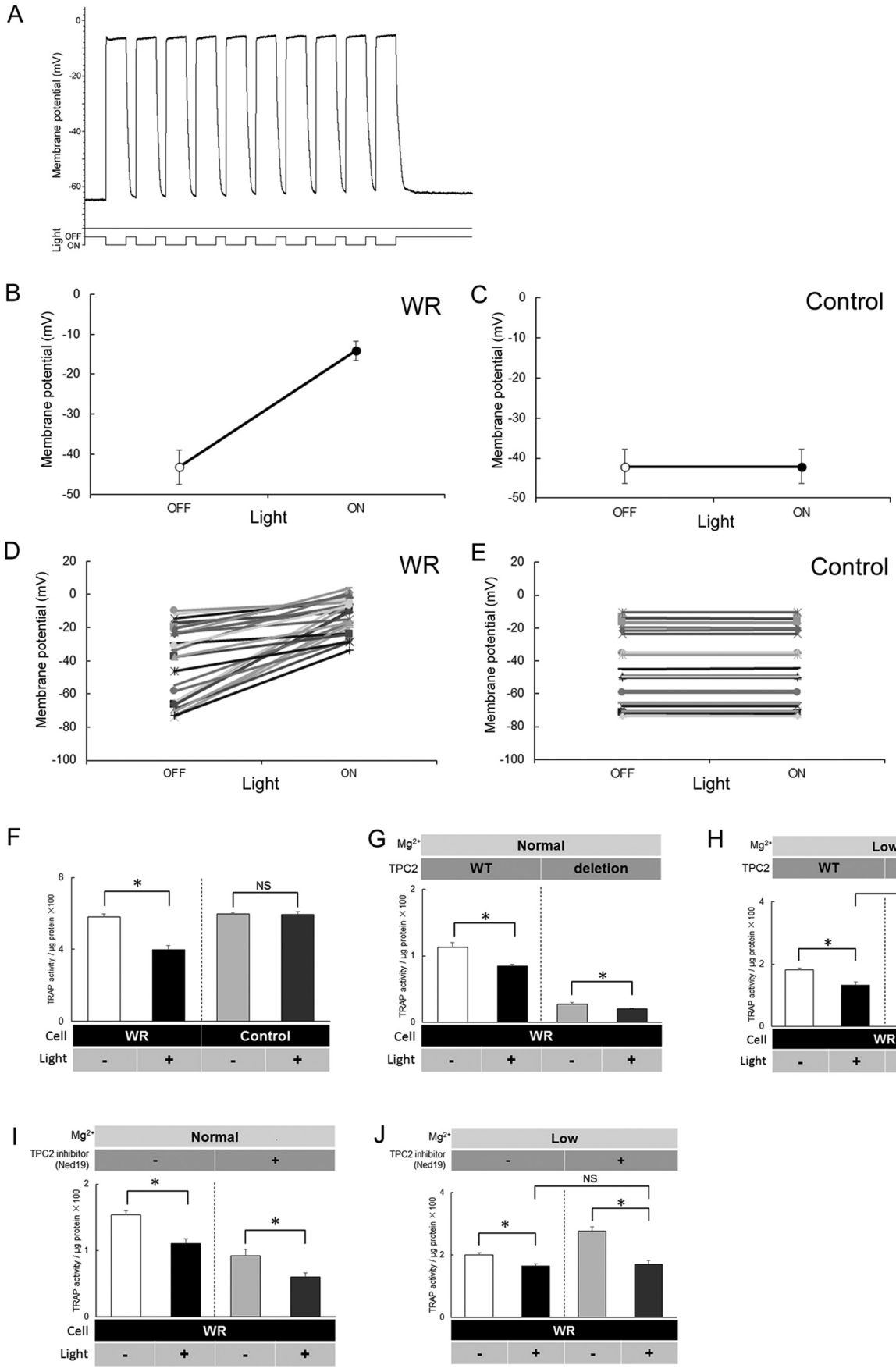
A
Membrane potential (mV)
0
-20
-40
-60
Light
OFF
ON
B
WR
Membrane potential (mV)
0
-10
-20
-30
-40
-50
OFF
Light
ON
C
Control
Membrane potential (mV)
0
-10
-20
-30
-40
-50
OFF
Light
ON
D
WR
Membrane potential (mV)
20
0
-20
-40
-60
-80
-100
OFF
Light
ON
E
Control
Membrane potential (mV)
20
0
-20
-40
-60
-80
-100
OFF
Light
ON
F
TRAP activity / μg protein ×100
8
4
0
*
NS
Cell
WR
Control
Light
-
+
-
+
G
Mg2+
Normal
TPC2
WT
deletion
TRAP activity / μg protein ×100
2
1
0
*
*
Cell
WR
Light
-
+
-
+
H
Mg2+
Low
TPC2
WT
deletion
TRAP activity / μg protein ×100
4
2
0
NS
*
*
Cell
WR
Light
-
+
-
+
I
Mg2+
Normal
TPC2 inhibitor (Ned19)
-
+
TRAP activity / μg protein ×100
2
1
0
*
*
Cell
WR
Light
-
+
-
+
J
Mg2+
Low
TPC2 inhibitor (Ned19)
-
+
TRAP activity / μg protein ×100
4
2
0
NS
*
*
WR
-
+
-
+

thoxy) phenylhydrazone, an inhibitor of ATP synthesis in the mitochondria, increased ~0.4 mM of $[Mg^{2+}]_i$ in PC12 cells. In another study (24), carbonyl cyanide *p*-(trifluoromethoxy) phenylhydrazone increased ~20–30% of the fluorescence intensity in KMG20-AM-loaded PC12 cells. Based on these reports and the linearity between KMG20 and concentration of Mg^{2+} (25), we estimated that the changes in 0.1 mM of $[Mg^{2+}]_i$ are equivalent to the changes in 5.0–7.5% of fluorescence intensity. In this study, the changes in fluorescence intensity by perfusion were found to be ~10–20% (supplemental Fig. S1*B*). We speculate that the $[Mg^{2+}]_i$ might be decreased by ~0.2 mM during osteoclastogenesis by low-Mg^{2+} condition. Jha *et al.* (16) showed that Mg^{2+} induced the functional conversion of TPC2 at 0.3 mM and inhibited TPC2 currents with an apparent affinity of 0.13 mM. Therefore, changes in $[Mg^{2+}]_i$ in low-Mg^{2+} culture medium could induce the functional conversion of TPC2, at least, in a part of the cells.

In animals and humans, the bone is the main storage site for both Mg^{2+} and Ca^{2+} (3, 4). Although molecular pathways of Ca^{2+} signaling in bone remodeling and bone cell physiology have been extensively investigated and are well understood, the molecules and signaling pathways related to Mg^{2+} remain unknown. Here, we identified TPC2 as a Mg^{2+}-dependent, functionally convertible molecule involved in osteoclastogenesis. Previous studies have shown that Mg^{2+} deficiency results in various, considerably different disorders, including osteoporosis (5, 26). Thus, our results could facilitate the discovery of molecular targets of the Mg^{2+} pathway. In osteoclast biology in particular, the mechanism underlying low-Mg^{2+}–induced osteoclastogenesis has remained unclear, but we now confirmed that Mg^{2+} deficiency-related osteoclastogenesis includes an inhibitory mechanism involving TPC2.

In this study, *myo*-inositol supplementation positively affected bone remodeling under low-Mg^{2+} conditions. A few previous studies have demonstrated beneficial effects of *myo*-inositol on the bone. *myo*-Inositol supplementation was reported to increase the Ca^{2+} uptake in the bone (27), and a mixture of arginine, inositol, and silicone was shown to increase the bone mineral density and strength (28, 29). Trabecular bone loss and reduced bone formation were observed in sodium/*myo*-inositol cotransporter knock-out mice, in which *myo*-inositol was not detected in cells, although the osteoclast numbers did not change (30). Here, *myo*-inositol supplementation affected the bone mass and osteoclastogenesis *in vivo* and *in vitro* only under low-Mg^{2+} conditions. Thus, *myo*-inositol likely exerts beneficial effects on bone remodeling under abnormal conditions such as Mg^{2+} deficiency. We did not detect any effect of *myo*-inositol supplementation on the bone under normal conditions. To elucidate the beneficial effects of *myo*-inositol, comparatively longer supplementation periods and further investigation are required.

TPC2 was suggested as a possible target molecule for osteoporosis treatment in our previous study (10). However, this suggestion must be revised based on the new findings of the complex mode of TPC2 action in this study, in which TPC2 showed distinct behaviors under normal- and low-Mg^{2+} conditions. Thus, TPC2 inhibition might not only suppress but also promote osteoclastogenesis, in particular, under conditions of Mg^{2+} deficiency, such as alcohol abuse, diabetes, and severe diarrhea (3). The functional conversion of TPC2 is related to MAPKs such as p38/JNK (16). Although we did not investigate the relationship between TPC2 and p38/JNK in osteoclast differentiation, future studies focused on TPC2 inhibition/activation *in vivo* for targeting bone diseases should involve the MAPK pathway.

In summary, our results demonstrated a different role of TPC2 in osteoclasts under low-Mg^{2+} conditions compared with that played under normal Mg^{2+} conditions. TPC2 regulated the low-Mg^{2+}–induced osteoclast differentiation in a manner distinct from that observed under normal conditions. Moreover, $PI(3,5)P_2$ inhibited osteoclastogenesis through TPC2 and membrane potential changes only under low-Mg^{2+} conditions. Meanwhile, *myo*-inositol, which can increase the $PI(3,5)P_2$ levels, rescued the low-Mg^{2+} diet–induced trabecular bone loss and concomitantly inhibited the increase in bone resorption. These new findings related to the Mg^{2+}-dependent role of osteoclastic TPC2 and to that of $PI(3,5)P_2$ highlight a previously unrecognized aspect of lysosomal biology and skeletal disorders.

Experimental procedures

Cell culture

RAW 264.7 mouse osteoclast precursor-like cells (American Type Culture Collection, Manassas, VA) were cultured in DMEM (GE Healthcare) supplemented with 10% FBS and 1% penicillin and streptomycin. To investigate the effects of Mg^{2+} on osteoclastogenesis, we used Mg^{2+}-free DMEM (GE Healthcare) with/without 1 mM $MgCl_2$. Moreover, to avoid any effects of FBS-derived Mg^{2+}, Mg^{2+}-free DMEM containing a reduced amount of FBS (2.5%) was used for osteoclast development (normal/low-Mg^{2+} media: Mg^{2+}-free DMEM containing 2.5% FBS with/without 1 mM $MgCl_2$, respectively). All cells were maintained at 37 °C and 5% CO_2 in a humidified atmosphere. All chemicals were purchased from Wako Pure Chemical Industries (Osaka, Japan) unless noted otherwise.

For osteoclast differentiation, RAW 264.7 cells were seeded at 2.0×10^5 cells/cm^2 with the addition of soluble RANKL

Figure 3. TPC2 is associated with membrane depolarization-induced inhibition of osteoclastogenesis. *A*, representative changes in membrane potential induced by a blue-light stimulus. Membrane depolarization occurred when the light was switched on and was terminated when the light was switched off. *B* and *C*, averaged light-induced depolarization. The light stimulus depolarized WR cells expressing channel rhodopsin-wide receiver-mCherry (*B*) but not control cells expressing mCherry only (*C*). *D* and *E*, single-cell depolarization by the light stimulus; each *line* represents a recorded cell. The light stimulus depolarized each single WR cell (*D*) but not single control cells (*E*). *F*, TRAP activity in control and WR cells in the presence (+) or absence (−) of light stimulation. The blue-light stimulus was applied every 12 h; TRAP activity decreased in WR cells at 3 days after the addition of RANKL ($n = 9$). *, $p < 0.01$; *NS*, not significant. *G* and *H*, TRAP activity in WR-expressing TPC2-WT and TPC2-deletion cells in the presence (+) or absence (−) of light stimulation under normal-Mg^{2+} (*G*) and low-Mg^{2+} (*H*) conditions. The blue-light stimulus was applied every 12 h ($n = 9$). *, $p < 0.01$; *NS*, not significant. *I* and *J*, TRAP activity in WR cells in the presence (+) or absence (−) of light stimulation and TPC2 inhibition under normal-Mg^{2+} (*G*) and low-Mg^{2+} (*H*) conditions. The blue-light stimulus was applied every 12 h ($n = 9$). *, $p < 0.01$; *NS*, not significant.

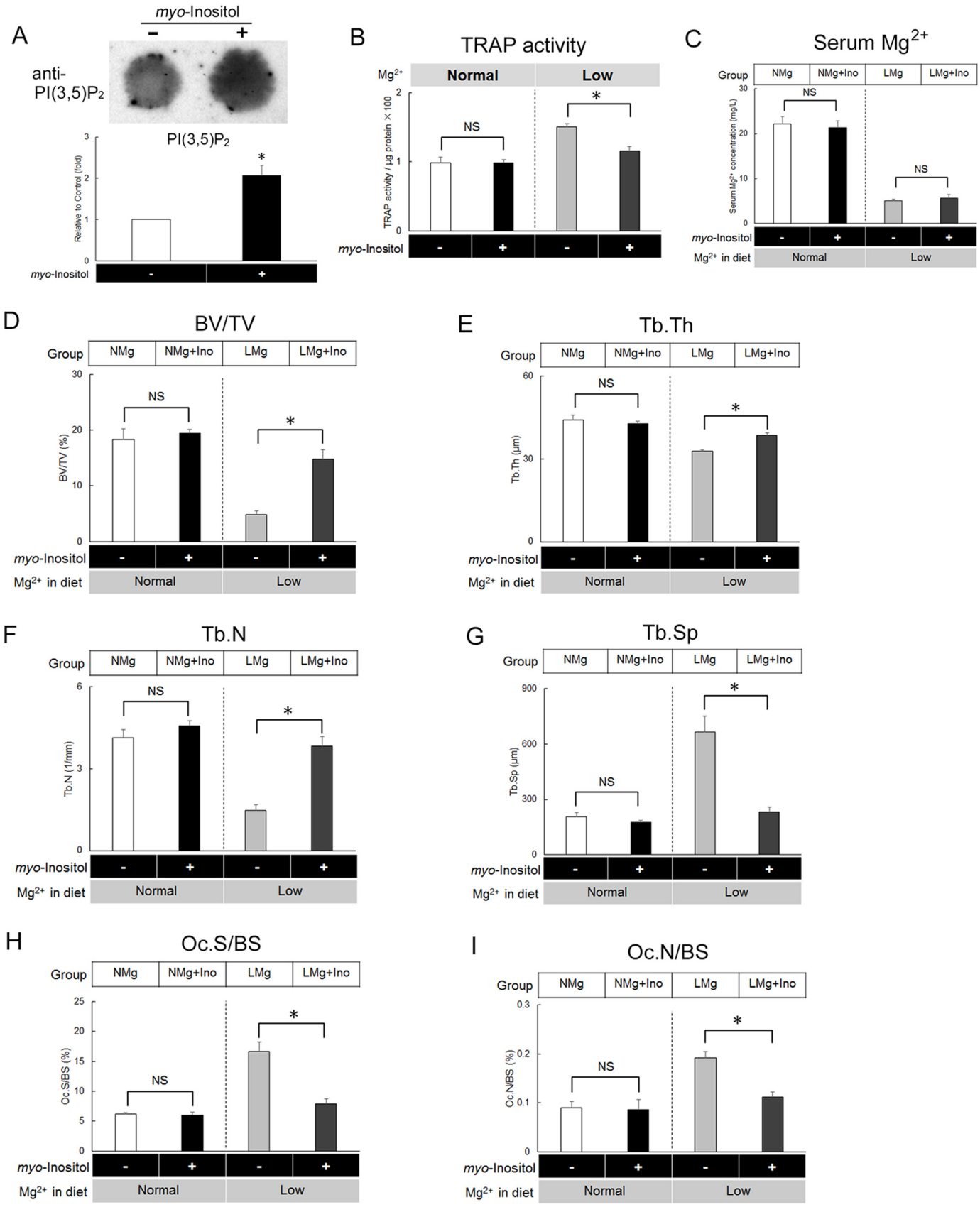
A
myo-Inositol
-
+
anti-
PI(3,5)P2
PI(3,5)P2
Relative to Control (fold)
*
myo-Inositol
B
TRAP activity
Mg2+
Normal
Low
TRAP activity / μg protein × 100
NS
*
myo-Inositol
C
Serum Mg2+
Group
NMg
NMg+Ino
LMg
LMg+Ino
Serum Mg2+ concentration (mg/L)
NS
myo-Inositol
Mg2+ in diet
Normal
Low
D
BV/TV
BV/TV (%)
E
Tb.Th
Tb.Th (μm)
F
Tb.N
Tb.N (1/mm)
G
Tb.Sp
Tb.Sp (μm)
H
Oc.S/BS
Oc.S/BS (%)
I
Oc.N/BS
Oc.N/BS (%)

(sRANKL, 50 ng/ml; Oriental Yeast, Tokyo, Japan). TRAP staining was performed as previously described (2, 10). Ned19 (1 μM; Tocris Bioscience, Bristol, UK), a TPC2 inhibitor, and YM201636 (100 nM; Tocris Bioscience), a PIKfyve inhibitor, were added to culture media in some experiments. For control, the same amount of DMSO was added. The shuttle PIP kit (catalog no. P-9035; Echelon Biosciences, Salt Lake City, UT) was used to add $PI(3,5)P_2$ (5 μM) to investigate the relationship between $PI(3,5)P_2$ and TPC2 under low-Mg^{2+} conditions. In the $PI(3,5)P_2$ experiments, the medium was replaced 2 h after the addition of $PI(3,5)P_2$ to avoid cell toxicity. Carrier3 (5 μM; Echelon Biosciences) was used to deliver $PI(3,5)P_2$ into the cells. For the control, the same amount of PBS was added with Carrier3. TRAP-positive cells with more than three nuclei were defined as multinucleated osteoclasts. Cells were cultured in 3.5-cm dishes by subculturing from 10-cm dishes. Samples were extracted from each 3.5-cm dish. This procedure was carried out three times at different time points.

Bone marrow–derived osteoclasts

Mouse bone marrow cells were obtained from the tibia and femur (C57BL/6 mice, 4-week-old males; Charles River Japan, Kanagawa, Japan). Bone marrow stromal cells were depleted from the mouse bone marrow by using a Sephadex G10 (GE Healthcare) column as previously described (2, 10). The obtained cells were cultured in Mg^{2+}-free DMEM with/without 1 mM $MgCl_2$ in the presence of macrophage colony-stimulating factor (50 ng/ml; R&D Systems, Minneapolis, MN) and sRANKL (50 ng/ml).

Establishment of cell lines

Cell lines were established as previously described (2, 10, 17). Lentiviral constructs expressing two different artificial guide RNAs, targeting murine TPC2 (target sequence: 5′-GAACGCCTGGCTCTCGCGGC-3′) and non-targeting gRNA, were prepared in a plasmid (lentiCRISPR v2 (one-vector system), a gift from Feng Zhang (Addgene plasmid catalog no. 52961)). This plasmid contains two expression cassettes, hSpCas9 and the chimeric guide RNA. Lentiviral constructs expressing WR or mCherry (control) were generated using the pLenti6.3/V5-DEST vector (Thermo Fisher Scientific). Viral transduction was performed as previously described (10). Briefly, lentiviral vectors and three packaging plasmids (pVSVG, pLG1, and pLG2) were transfected into 293FT cells using Lipofectamine 2000 (Thermo Fisher Scientific), and the culture medium (lentiviral solution) was collected after 48 h. Viral titers were estimated using Lenti-X quantitative reverse transcription-PCR (Chemicon, Temecula, CA). Viral transduction was performed by adding the lentiviral solution to the culture medium in the presence of 6 μg/ml Polybrene (Sigma–Aldrich). For guide RNA-expressing cells, puromycin (5 μg/ml) was added to the culture medium for 3 days. Then TPC2-deficient cell clones were selected by limited dilution. Stably transduced cells expressing WR or mCherry were selected using 5 μg/ml blasticidin (Thermo Fisher Scientific).

Light stimulus experiment for osteoclast differentiation

The light stimulus experiment has been described previously (2, 17). The light stimulus (480 ± 10 nm, 2-s stimulus followed by a 1-s rest, repeated 10 times) was applied to cells under an IX71 inverted microscope (Olympus, Tokyo, Japan) equipped with a VMM-T1 fluorescence shutter controller (Uniblitz, Rochester, NY). RAW cells stably expressing WR or control cells (mCherry only) were used for the light stimulus experiments. Both WR and control cells were seeded at 2.0×10^6 cells/cm^2, and the experiment was repeated three times.

Measurement of Mg^{2+} concentration and TRAP activity

To measure the Mg^{2+} concentration, the cells were quickly rinsed with cold PBS, and a cell lysate was obtained with a solution containing 50 mM Tris-HCl (pH 7.4) and 1% Nonidet P-40. Magnesium concentrations were determined using a magnesium test (Wako) according to the manufacturer's protocol.

TRAP activity was measured as previously described (2, 10, 17). Briefly, cells were lysed in extraction buffer (150 mM NaCl, 50 mM Tris, 1% Nonidet P-40, pH 8.0) supplemented with protease inhibitors (Sigma–Aldrich), and a 20-μl aliquot of the lysate was added to 200 μl of TRAP buffer (50 mM sodium acetate, 25 mM sodium tartrate, 0.4 mM $MnCl_2$, 0.4% *N*,N-dimethylformamide, 0.2 mg/ml Fast Red Violet, 0.5 mg/ml naphthol AS-MX phosphate, pH 5.0). After incubation for 1 h (BM) or 2 h (RAW) at 37 °C, absorbance was measured at 540 nm using a SpectraMax microplate reader (Molecular Devices, Sunnyvale, CA). The data were normalized to the total protein content, which was determined using a bicinchoninic acid kit (Thermo Fisher Scientific). Each experiment was performed in triplicate.

Gene expression assay

Total RNA was extracted using an RNeasy kit (Qiagen) according to the manufacturer's protocol. First-strand cDNA was synthesized from total RNA using a high-capacity cDNA reverse transcription kit (Thermo Fisher Scientific). The amount of total RNA used in each reaction of synthesis was 1 μg. Quantitative real-time PCR was performed using a StepOne real-time PCR system (Thermo Fisher Scientific), SYBR Green (Fast SYBR Green master mix, Thermo Fisher Scientific), and specific forward and reverse primers. According to the manufacturer's protocol, the conditions for the reaction were 20 μl/well, including 10 μl of SYBR Green, 1.0 μl of cDNA tem-

Figure 4. *myo*-Inositol supplementation reverses low-Mg^{2+}–induced bone loss and inhibits osteoclastogenesis. *A*, quantification of $PI(3,5)P_2$ levels in total cell lysates of RAW cells, based on dot-blot analysis. $PI(3,5)P_2$ levels increased at 24 h after the *myo*-inositol addition ($n = 9$). *, $p < 0.01$. *B*, TRAP activity in the presence (+) or absence (−) of *myo*-inositol in normal- and low-Mg^{2+} RAW cell cultures at 3 days after the addition of RANKL ($n = 9$). *, $p < 0.01$; *NS*, not significant. *C*, serum Mg^{2+} concentrations in the experimental groups at the end of the experiment ($n = 4$ each). A low-Mg^{2+} diet reduced the serum Mg^{2+} concentrations with/without *myo*-inositol supplementation. *NS*, not significant. *D–G*, structural parameters of the femur, BV/TV (*D*), Tb.Th (*E*), Tb.N (*F*), and Tb.Sp (*G*), based on microcomputed tomography analysis. *myo*-Inositol supplementation affected all structural parameters only with the low-Mg^{2+} diet (LMg *versus* LMg+Ino; $n = 4$, each). *, $p < 0.01$; *NS*, not significant. *H* and *I*, resorption parameters of the femur: Oc.S/BS (*H*) and Oc.N/BS (*I*). *myo*-Inositol supplementation inhibited low-Mg^{2+}–induced bone resorption ($n = 4$). *, $p < 0.01$; *NS*, not significant.

plate, 0.15 μl of 100 μM forward and reverse primers, and 8.7 μl of RNase-free water. The thermal cycling conditions were as follows: 95 °C for 20 s, followed by 40 cycles of 95 °C for 3 s and 60 °C for 30 s. Transcript levels were normalized relative to those of glyceraldehyde-3-phosphate dehydrogenase (*GAPDH*). The quantitative analysis was automatically performed by the StepOne software (Thermo Fisher Scientific). The forward and reverse primer sequences were as follows: calcitonin receptor (GenBank™ accession number BC119272.1), 5′-GCCAGCCGCCCAAGACTCTG-3′ and 5′-GGCAGGGTGAGGCGCAGAAG-3′; integrin β3 (GenBank™ accession number NM_016780.2), 5′-GACAGGATGCGAGCGCAGTG-3′ and 5′-AGTTCACGCCTCGTGTGGTA-3′; cathepsin K (GenBank™ accession number NM_007802.4), 5′-TTCTCCTCTCGTTGGTGCTT-3′ and 5′-AAAAATGCCCTGTTGTGTCC-3′; and *GAPDH* (GenBank™ accession number GU214026.1), 5′-AGAAGGTGGTGAAGCAGGCAT-3′ and 5′-CGAAGGTGGAAGAGTGGGAGTTG-3′. The *GAPDH* signals showed no differences among the experimental groups (supplemental Fig. S2*A*).

Fluorescence-based recording of $[Ca^{2+}]_i$, $[Na^+]_i$, $[Mg^{2+}]_i$, and membrane potential

Fluorescence-based recording of membrane potential has been described elsewhere (2, 17). Cells were loaded with the FLIPR dye (FLIPR membrane assay kit; Molecular Devices) for 30 min in Hanks' balanced salt solution (HBSS) containing 1 mM $CaCl_2$ with/without 1 mM $MgCl_2$ at 37 °C and 5% CO_2 in a humidified incubator. The membrane potential was recorded every 30 s for 120 min using a FLIPR Tetra system (Molecular Devices) at room temperature. To analyze the changes in membrane potential, fluorescence intensity in each well was quantified using the FLIPR software (Molecular Devices).

The protocol for recording $[Na^+]_i$, $[Ca^{2+}]_i$, and $[Mg^{2+}]_i$ was described previously (2, 17, 24). Briefly, the cells were loaded with 5 μM CoroNa (Thermo Fisher Scientific) for $[Na^+]_i$, Fluo8-AM (Nacalai Tesque, Kyoto, Japan) for $[Ca^{2+}]_i$, and 10 μM KMG-20-AM (Wako) for $[Mg^{2+}]_i$ for 30 min in HBSS containing 1 mM $CaCl_2$ with/without 1 mM $MgCl_2$ at 37 °C and 5% CO_2 in a humidified incubator. After rinsing the cells, the images were captured every 30 s for 120 min for $[Na^+]_i$ and $[Ca^{2+}]_i$ using a SpectraMax fluorescence microplate reader. To analyze the changes in $[Na^+]_i$ and $[Ca^{2+}]_i$ in each well, the fluorescence intensity was quantified using the SoftMax Pro software (Molecular Devices). The replacement experiments for $[Na^+]_i$ were initiated after the incubation with physiological solution containing 145 mM NaCl, 5 mM KCl, 1 mM $CaCl_2$, 1 mM $MgCl_2$, 10 mM D-glucose, 0.1% BSA, and 10 mM HEPES (pH 7.4). To confirm the effects of Na^+, NaCl was replaced with *N*-methyl-D-glucamine chloride (supplemental Fig. S2*G*). For $[Mg^{2+}]_i$, images were captured every 6 s for 400 s using an LSM700 confocal fluorescence microscope (Carl Zeiss). HBSS (2.0 ml) was continuously perfused with/without $MgCl_2$ at a rate of 4–5 ml/min. Exchange of the solutions could be accomplished within 30 s. To analyze $[Mg^{2+}]_i$ changes in individual cells, the fluorescence intensity was quantified using the LSM image software (Carl Zeiss). Approximately five to seven cells per field were analyzed in each culture, and the experiment was repeated several times. The experiments were initiated after incubation of HBSS at room temperature for 5–10 min. $PI(3,5)P_2$ with Carrier3 or PBS with Carrier3 were added to the solution. At the end of the experiment, cell viability was confirmed by adding a 150 mM KCl solution (for membrane potential) and 5 μM ionomycin (for $[Na^+]_i$ and $[Ca^{2+}]_i$) (supplemental Fig. S2, *C–E*).

Electrophysiology

Electrophysiological experiments were performed as previously described (2, 17). For whole-cell recordings, the standard external solution contained 145 mM NaCl, 5 mM KCl, 1 mM $CaCl_2$, 1 mM $MgCl_2$, 10 mM glucose, 10 mM HEPES (pH 7.3), and 0.1% bovine serum albumin. The pipette solution contained 130 mM potassium gluconate, 20 mM KCl, 3 mM $MgCl_2$, 1 mM EGTA, 1 mM ATP, 0.5 mM GTP, and 10 mM HEPES (pH 7.3). The pH levels of the bath and pipette solutions were adjusted with NaOH and KOH. The osmolality of the solution without $CaCl_2$, $MgCl_2$, glucose, and BSA or ATP and GTP was determined using a micro-osmometer type 13 (Roebling, Berlin, Germany). The osmolality of this solution was 280–300 mOsm. The external and internal solutions with $CaCl_2$, $MgCl_2$, glucose, and BSA for the external solution or ATP and GTP for the internal solution had osmolalities of 320–330 and 290–300 mOsm, respectively.

The resistance of the used borosilicate glass pipettes was 5–8 MΩ. The reference electrode was an Ag-AgCl wire connected to the bath solution through a Ringer-agar bridge. The zero current potential before the formation of the gigaseal was taken as 0 mV. The current signals were recorded using an Axopatch 200A amplifier (Axon Instruments, Foster City, CA) digitized at 1–2 kHz with a Digidata 1200 analog-digital converter (Axon Instruments) and analyzed using the pCLAMP software (Axon Instruments). The membrane potential was recorded in the current-clamp mode.

Western blotting and quantification of $PI(3,5)P_2$ levels

The cells were rinsed with cold phosphate-buffered saline, and total protein was extracted with a solution containing 50 mM Tris-HCl (pH 7.4) and 1% Triton X-100. Protease inhibitors (Wako) were added to all solutions. Total protein was extracted from the entire tibia as described previously (31), and the protein concentration was determined using a bicinchoninic acid assay kit. SDS-PAGE was performed as previously described (32). Briefly, proteins were separated in 7.0% gels and transferred to polyvinylidene difluoride membranes. The membranes were blocked with EzBlock (Atto, Tokyo, Japan) and incubated with an antibody against TPC2 (1:2,000; Alomone Labs, Jerusalem, Israel) or with the antibody preincubated with an antigen (10 μg/ml; control peptide antigen for anti-TPC2; Alomone Labs). The antibody was incubated with the antigen for 1–2 h at room temperature. The quantity of total protein loaded to each lane was adjusted to 10 μg. For quantification of $PI(3,5)P_2$ levels, 10 μl of the lysate was pipetted onto a nitrocellulose membrane. The quantity of total protein for each dot was adjusted to 10 μg. To confirm the linearity of the signal intensity, $PI(3,5)P_2$ (range, 0.031–2.0 nmol/dot) was pipetted onto the membrane. After drying, the membrane was blocked with

EzBlock and then incubated with an anti-$PI(3,5)P_2$ antibody (1:1,000; Echelon Biosciences). Images were captured using a CCD camera (ChemiDoc; Bio-Rad), and quantitative analysis was performed using the Image Lab software (Bio-Rad).

Animals

Sixteen 3-week-old male C57BL/6J mice (Charles River Japan) were allowed to acclimate for 1 week at 22 ± 2 °C and 60% humidity under a 12/12-h light/dark cycle (with light exposure from 7:00 a.m. to 7:00 p.m.). Drinking water with/without *myo*-inositol (Ino: 10 mg/ml) was available at all times, and the rats were fed a NMg or LMg (CLEA Japan, Tokyo, Japan), with the magnesium content of 80 mg/100 g (NMg) and 2.7 mg/100 g (LMg). The body weight of the mice was measured weekly, and all mice were found to remain healthy.

The mice were divided into four groups of four animals each at the age of 4 weeks as follows. Groups NMg and NMg+Ino received the NMg diet and NMg diet with drinking water containing Ino, respectively. Groups LMg and LMg+Ino received the LMg diet and LMg diet with drinking water containing Ino, respectively. The mice were sacrificed at the age of 8 weeks through exsanguination under ether anesthesia. All studies involving animals were performed in accordance with the procedures approved by the Tokyo Medical and Dental University and Osaka Dental University Animal Care and Use Committees.

Microcomputed tomography

Microcomputed tomography analysis was performed as previously described (31). The 3D microcomputed tomography images were captured using an MX-90 3D system (Medixtech, Tokyo, Japan) and analyzed using the TRI/3D-Bon software (Ratoc System Engineering, Tokyo, Japan). The X-ray source was set at 90 kV and 90 μA for 3D imaging.

Bone histomorphometry

Bone histomorphometry was performed as previously described (33, 34). Femoral bone samples were embedded in a mixture of methyl methacrylate, hydroxyglycol methacrylate, and 2-hydroxyethylacrylate, which was polymerized at 4 °C. Sections were obtained and stained for TRAP. Histomorphometry was performed on a semiautomatic image analysis system connected to a light microscope (Cosmozone 1S; Nikon, Tokyo, Japan). For each section, the secondary spongiosa area was measured. We also measured the osteoclast surface area (μm) and number and trabecular BS (μm) as bone resorption parameters. TRAP-positive cells that formed resorption lacunae at the trabecular surface and contained three or more nuclei were identified as osteoclasts.

Statistical analysis

The values are expressed as the means ± S.E. of the mean, and all values were analyzed using the Student's *t* test or analysis of variance. The Tukey's honest significant difference test was applied as a post hoc test. $p < 0.05$ was considered statistically significant. Analyses were performed using SPSS (SPSS Japan, Tokyo, Japan).

Author contributions—T. Notomi, M. K., and M. N. designed the study. T. Notomi, M. K., A. H., and T. Nozaki performed the study and collected the data. T. Notomi, M. K., A. H., K. O., Y. E., and M. N. analyzed the data. T. Notomi, M. K., Y. E., and M. N. wrote the paper.

References

1. Nieves, J. W. (2013) Skeletal effects of nutrients and nutraceuticals, beyond calcium and vitamin D. *Osteoporos. Int.* **24,** 771–786
2. Notomi, T., Kuno, M., Hiyama, A., Ohura, K., Noda, M., and Skerry, T. M. (2015) Zinc-induced effects on osteoclastogenesis involves activation of hyperpolarization-activated cyclic nucleotide modulated channels via changes in membrane potential. *J. Bone Miner. Res.* **30,** 1618–1626
3. Swaminathan, R. (2003) Magnesium metabolism and its disorders. *Clin. Biochem. Rev.* **24,** 47–66
4. Parfitt, A. M., and Kleerekoper, M. (1980) *Clinical Disorders of Calcium, Phosphorus and Magnesium Metabolism*, 3rd Ed. (Maxwell, M. H., and Kleeman, C. R., eds), pp. 947–960, McGraw-Hill, New York
5. Castiglioni, S., Cazzaniga, A., Albisetti, W., and Maier, J. A. (2013) Magnesium and osteoporosis: current state of knowledge and future research directions. *Nutrients* **5,** 3022–3033
6. Belluci, M. M., Schoenmaker, T., Rossa-Junior, C., Orrico, S. R., de Vries, T. J., and Everts, V. (2013) Magnesium deficiency results in an increased formation of osteoclasts. *J. Nutr. Biochem.* **24,** 1488–1498
7. Boyle, W. J., Simonet, W. S., and Lacey, D. L. (2003) Osteoclast differentiation and activation. *Nature* **423,** 337–342
8. Karsenty, G., and Wagner, E. F. (2002) Reaching a genetic and molecular understanding of skeletal development. *Dev. Cell* **2,** 389–406
9. Takayanagi, H., Kim, S., Koga, T., Nishina, H., Isshiki, M., Yoshida, H., Saiura, A., Isobe, M., Yokochi, T., Inoue, J., Wagner, E. F., Mak, T. W., Kodama, T., and Taniguchi, T. (2002) Induction and activation of the transcription factor NFATc1 (NFAT2) integrate RANKL signaling in terminal differentiation of osteoclasts. *Dev. Cell.* **3,** 889–901
10. Notomi, T., Ezura, Y., and Noda, M. (2012) Identification of two-pore channel 2 as a novel regulator of osteoclastogenesis. *J. Biol. Chem.* **287,** 35057–35064
11. Calcraft, P. J., Ruas, M., Pan, Z., Cheng, X., Arredouani, A., Hao, X., Tang, J., Rietdorf, K., Teboul, L., Chuang, K. T., Lin, P., Xiao, R., Wang, C., Zhu, Y., Lin, Y., *et al.* (2009) NAADP mobilizes calcium from acidic organelles through two-pore channels. *Nature* **459,** 596–600
12. Galione, A., Morgan, A. J., Arredouani, A., Davis, L. C., Rietdorf, K., Ruas, M., and Parrington, J. (2010) NAADP as an intracellular messenger regulating lysosomal calcium-release channels. *Biochem. Soc. Trans.* **38,** 1424–1431
13. Wang, X., Zhang, X., Dong, X.-P., Samie, M., Li, X., Cheng, X., Goschka, A., Shen, D., Zhou, Y., Harlow, J., Zhu, M. X., Clapham, D. E., Ren, D., and Xu, H. (2012) TPC proteins are phosphoinositide- activated sodium-selective ion channels in endosomes and lysosomes. *Cell.* **151,** 372–383
14. Guo, J., Zeng, W., and Jiang, Y. (2017) Tuning the ion selectivity of two-pore channels. *Proc. Natl. Acad. Sci. U.S.A.* **114,** 1009–1014
15. Cang, C., Zhou, Y., Navarro, B., Seo, Y.-J., Aranda, K., Shi, L., Battaglia-Hsu, S., Nissim, I., Clapham, D. E., and Ren, D. (2013) mTOR regulates lysosomal ATP-sensitive two-pore Na^+ channels to adapt to metabolic state. *Cell* **152,** 778–790
16. Jha, A., Ahuja, M., Patel, S., Brailoiu, E., and Muallem, S. (2014) Convergent regulation of the lysosomal two-pore protein kinases. *EMBO J.* **33,** 501–511
17. Notomi, T., Kuno, M., Hiyama, A., Ezura, Y., Honma, M., Ishizuka, T., Ohura, K., Yawo, H., and Noda, M. (2015) Membrane depolarization regulates intracellular RANKL transport in non-excitable osteoblasts. *Bone* **81,** 306–314
18. Clements, R. S., Jr., and Darnell, B. (1980) *myo*-Inositol content of common foods: development of a high-*myo*-inositol diet. *Am. J. Clin. Nutr.* **33,** 1954–1967
19. Zolov, S. N., Bridges, D., Zhang, Y., Lee, W. W., Riehle, E., Verma, R., Lenk, G. M., Converso-Baran, K., Weide, T., Albin, R. L., Saltiel, A. R., Meisler,

M. H., Russell, M. W., and Weisman, L. S. (2012) *In vivo*, PIKfyve generates PI(3,5)P2, which serves as both a signaling lipid and the major precursor for PI5P. *Proc. Natl. Acad. Sci. U.S.A.* **109,** 17472–17477

20. Pitt, S. J., Funnell, T. M., Sitsapesan, M., Venturi, E., Rietdorf, K., Ruas, M., Ganesan, A., Gosain, R., Churchill, G. C., Zhu, M. X., Parrington, J., Galione, A., and Sitsapesan, R. (2010) TPC2 is a novel NAADP-sensitive Ca^{2+} release channel, operating as a dual sensor of luminal pH and Ca^{2+}. *J. Biol. Chem.* **285,** 35039–35046
21. Zhu, M. X., Ma, J., Parrington, J., Galione, A., and Evans, A. M. (2010) TPCs: Endolysosomal channels for Ca2+ mobilization from acidic organelles triggered by NAADP. *FEBS Lett.* **584,** 1966–1974
22. Romani, A. M., and Scarpa, A. (2000) Regulation of cellular magnesium. *Front. Biosci.* **5,** D720–D734
23. Shindo, Y., Yamanaka, R., Suzuki, K., Hotta, K., and Oka, K. (2015) Intracellular magnesium level determines cell viability in the MPP^+ model of Parkinson's disease. *Biochim. Biophys. Acta* **1853,** 3182–3191
24. Kubota, T., Tokuno, K., Nakagawa, J., Kitamura, Y., Ogawa, H., Suzuki, Y., Suzuki, K., and Oka, K. (2003) Na^+/Mg^{2+} transporter acts as a Mg^{2+} buffering mechanism in PC12 cells. *Biochem. Biophys. Res. Commun.* **303,** 332–336
25. Suzuki, Y., Komatsu, H., Ikeda, T., Saito, N., Araki, S., Citterio, D., Hisamoto, D., Kitamura, Y., Kubota, T., Nakagawa, J., Oka, K., and Suzuki, K. (2002) Design and synthesis of Mg^{2+}-selective fluoroionophores based on a coumarin derivative and application for Mg^{2+} measurement in a living cell. *Anal. Chem.* **74,** 1423–1428
26. Rude, R. K., Singer, F. R., and Gruber, H. E. (2009) Skeletal and hormonal effects of magnesium deficiency. *J. Am. Coll. Nutr.* **28,** 131–141
27. Angeloff, L. G., Skoryna, S. C., and Henderson, I. W. (1977) Effects of the hexahydroxyhexane myoinositol on bone uptake of radiocalcium in rats: effect of inositol and vitamin D2 on bone uptake of 45Ca in rats. *Acta Pharmacol. Toxicol.* (*Copenh.*) **40,** 209–215
28. Yaman, F., Acikan, I., Dundar, S., Simsek, S., Gul, M., Ozercan, I. H., Komorowski, J., and Sahin, K. (2016) Dietary arginine silicate inositol complex increased bone healing: histologic and histomorphometric study. *Drug Des. Devel. Ther.* **10,** 2081–2086
29. Seaborn, C. D., and Nielsen, F. H. (2002) Dietary silicon and arginine affect mineral element composition of rat femur and vertebra. *Biol. Trace Elem. Res.* **89,** 239–250
30. Dai, Z., Chung, S. K., Miao, D., Lau, K. S., Chan, A. W., and Kung, A. W. (2011) Sodium/myo-inositol cotransporter 1 and *myo*-inositol are essential for osteogenesis and bone formation. *J. Bone Miner. Res.* **26,** 582–590
31. Aryal A. C. S., Miyai, K., Izu, Y., Hayata, T., Notomi, T., Noda, M., and Ezura, Y. (2015) Nck influences preosteoblastic/osteoblastic migration and bone mass. *Proc. Natl. Acad. Sci. U.S.A.* **112,** 15432–15437
32. Notomi, T., and Shigemoto, R. (2004) Immunohistochemical localization of Ih channel subunits, HCN1–4, in the rat brain. *J. Comp. Neurol.* **471,** 241–276
33. Notomi, T., Karasaki, I., Okazaki, Y., Okimoto, N., Kato, Y., Ohura, K., Noda, M., Nakamura, T., and Suzuki, M. (2014) Insulinogenic sucrose+amino acid mixture ingestion immediately after resistance exercise has an anabolic effect on bone compared with non-insulinogenic fructose+amino acid mixture in growing rats. *Bone* **65,** 42–48
34. Notomi, T., Okimoto, N., Okazaki, Y., Tanaka, Y., Nakamura, T., and Suzuki, M. (2001) Effects of tower climbing exercise on bone mass, strength, and turnover in growing rats. *J. Bone Miner. Res.* **16,** 166–174